Naval Research Laboratory

Washington, DC 20375-5320

NRL/MR/6362--20-10,074

Novel Deposition Approaches of Self-Assembled Molecular Films – Towards Understanding of Formation of Two-Level Systems for Quantum Computing Applications

Evgeniya H. Lock

Materials and Sensors Branch
Materials Science and Technology Division

Zariana Mobley

Former SSEP-STEM Student
Materials Science and Technology Division

Stephen Deese

Former ASEE Postdoctoral Associate
Chemistry Division

Matthew Laskoski

Materials Chemistry Branch
Chemistry Division

August 13, 2020

REPORT DOCUMENTATION PAGE

Form Approved
OMB No. 0704-0188

1. REPORT DATE *(DD-MM-YYYY)*	2. REPORT TYPE	3. DATES COVERED *(From - To)*
13-08-2020	NRL Memorandum Report	01 Oct 2019 – 30 Sep 2020

4. TITLE AND SUBTITLE

Novel Deposition Approaches of Self-Assembled Molecular Films – Towards Understanding of Formation of Two-Level Systems for Quantum Computing Applications

5a. CONTRACT NUMBER

5b. GRANT NUMBER

5c. PROGRAM ELEMENT NUMBER

6. AUTHOR(S)

Evgeniya H. Lock, Zariana Mobley, Stephen Deese, and Matthew Laskoski

5d. PROJECT NUMBER

5e. TASK NUMBER

5f. WORK UNIT NUMBER
1G71

7. PERFORMING ORGANIZATION NAME(S) AND ADDRESS(ES)

Naval Research Laboratory
4555 Overlook Avenue, SW
Washington, DC 20375-5320

8. PERFORMING ORGANIZATION REPORT NUMBER

NRL/MR/6362--20-10,074

9. SPONSORING / MONITORING AGENCY NAME(S) AND ADDRESS(ES)

10. SPONSOR / MONITOR'S ACRONYM(S)

11. SPONSOR / MONITOR'S REPORT NUMBER(S)

12. DISTRIBUTION / AVAILABILITY STATEMENT

DISTRIBUTION STATEMENT A: Approved for public release; distribution is unlimited.

13. SUPPLEMENTARY NOTES

14. ABSTRACT

The progress in quantum technology relies on high performing qubits with minimal losses in superconducting and dielectric properties, as well as in their interfaces. Understanding what causes the loss of performance is of paramount importance. In this work, we focus on the development of chemical molecules that possess molecular rotors (CF-, OH- functional groups) in their structures that move at a particular microwave frequency. Tracking of these frequencies provides unprecedented insight into the loss mechanisms in lossy dielectric systems. The goal of this work is to develop deposition methods of self-assembled molecules onto hydrogen terminated Si surfaces using strong Si-C bonds for molecular attachment rather than the typical Si-O. In the first part of the report we discuss the synthesis and the deposition of w-F alkyne monolayers containing ten (C_{10}) and eighteen (C_{18}) carbon chains in their structure onto Si surfaces. We found that deposition of these molecules following established literature protocols did not produce uniform closely packed monolayers. Thus, we developed new deposition protocols and established critical parameters that needed attention for further process optimization. The second part of the report is devoted to the deposition of 4-(vinyl)phenol (VP), 3-(ethenyl)phenol (EP), and 4-(vinylphenol)methanol (VPM) onto Si surfaces. The most successful deposition was achieved with EP molecules which produced multilayer films with hydrophobic nature, followed by VP, and finally, VPM films. Further experiments with increased deposition temperature and catalyst are needed to optimize the developed protocols.

15. SUBJECT TERMS

Quantum technology
Molecular rotors
Self assembled monolayers
Two level systems

16. SECURITY CLASSIFICATION OF:			17. LIMITATION OF ABSTRACT	18. NUMBER OF PAGES	19a. NAME OF RESPONSIBLE PERSON
a. REPORT	b. ABSTRACT	c. THIS PAGE			Evgeniya H. Lock
Unclassified Unlimited	Unclassified Unlimited	Unclassified Unlimited	Unclassified Unlimited	31	19b. TELEPHONE NUMBER *(include area code)* (202) 767-0351

Standard Form 298 (Rev. 8-98)
Prescribed by ANSI Std. Z39.18

This page intentionally left blank.

1 Objective

The objectives of this work are

1) To deposit ω-F alkyne monolayers containing C_{10} and C_{18} carbon chains in their structure and characterize deposition quality.
2) To deposit 4-(vinyl)phenol (VP), 3-(ethenyl)phenol (EP), and 4-(vinylphenol)methanol (VPM) on hydrogen terminated Si surface and characterize deposition quality.

2 Approach

Two level systems (TLS) are the relevant source of decoherence in superconducting qubits[1]. They are found in Josephson junction tunneling barriers, insulating films, and native oxides on surfaces. One way to control TLS is by intentionally preparing different vacuum-dielectric and dielectric-superconducting interfaces for improvements[2]. Another approach relies on preparing molecules as potential TLS on surfaces and then modifying them to improve Q-factor. The TLS behavior is controlled by the dipole moment and surface coverage of the molecules.

The current state of the art is focused on characterization of dipole moments of TLS in deposited films[3,4]. The goal of this work is to develop deposition methods of self-assembled molecules onto H-terminated Si surfaces to avoid the influence of the Si-O substrate functional groups (Figure 1). The attachment of the molecules to H-terminated Si happens through Si-C bond formation through heat[5,6] or light[7], however, the deposition protocols and surface coverage vary widely. In our work, we followed the protocols outlined by Pujani *et. al.* [6] with slight modifications that will be explained below.

Manuscript approved May 11, 2020.

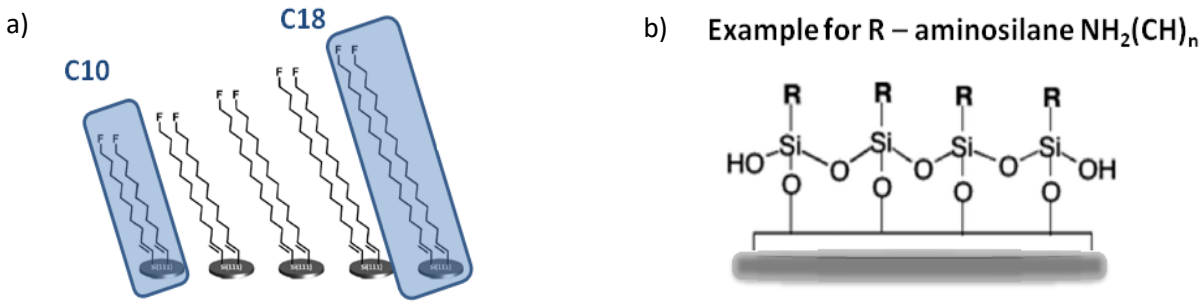

Figure 1. Comparison between ω-F alkyne monolayers containing ten (C_{10}) and eighteen (C_{18}) carbon chains (a) and silane-based monolayers used for Si surface functionalization

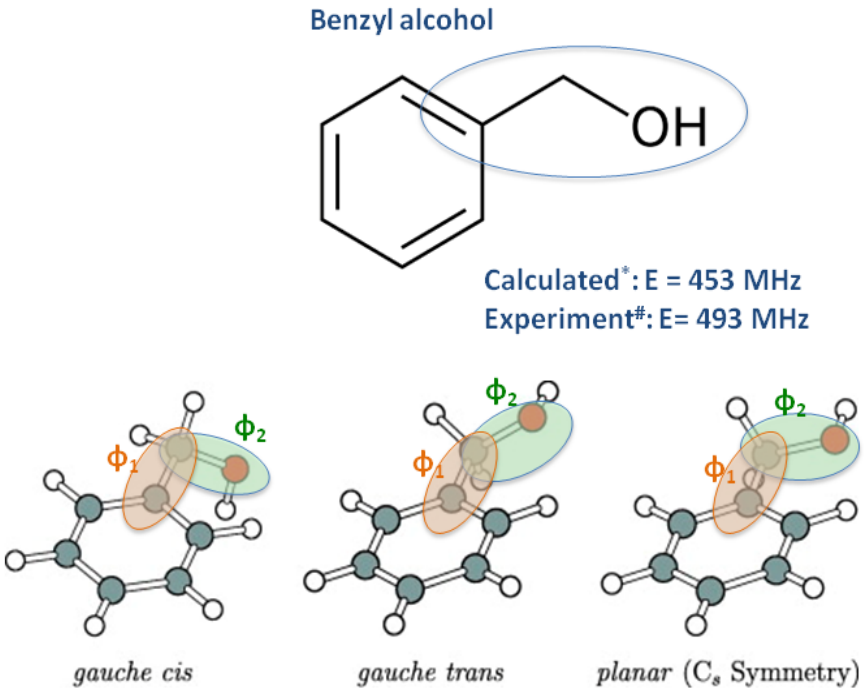

Figure 2. Theoretically predicted and experimentally observed rotation of -OH functionality in benzyl alcohol[8 9]

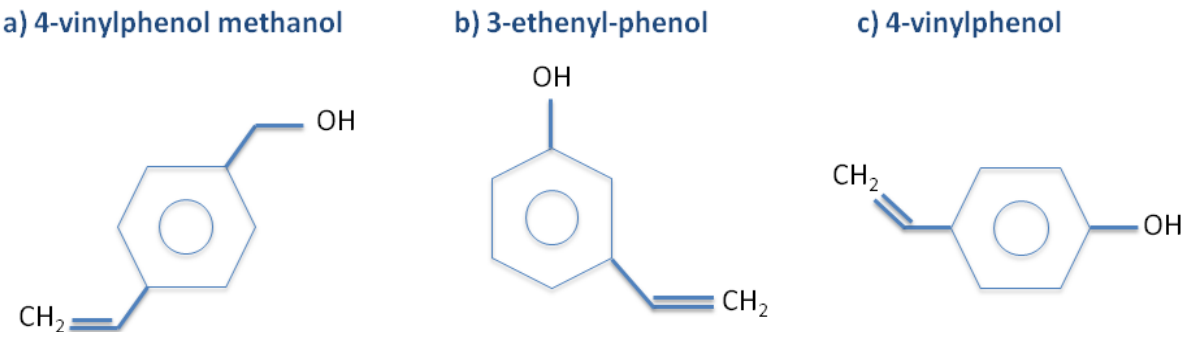

Figure 3. Molecular rotor structures: VPM (a), EP (b) and VP (c)

In the fields of pulsed-jet Fourier transform microwave and free-jet absorption millimeter wave spectroscopy, rotational spectrum, tunneling motion and potential barriers of different molecules have been experimentally measured, and, using ab-initio calculations, theoretically predicted[8,9]. Of particular interest for this study is benzyl alcohol shown in Figure 2, as this molecule has four minima and splitting energy of 490 MHz, thus making it an ideal candidate for molecular rotor motion detection at mili-Kelvin temperatures. However, in the above sited literature the molecules are dispersed in the jet, while in the experiment that we envision the molecules will be deposited onto the Si surface of the resonator. To achieve attachment of this molecule we will use the same Si-C bond attachment scheme as outlined above. The three candidate molecules that we selected are shown in Figure 3. They have nominally the same structure – however the position of -OH, and -CH_2OH functional groups with respect to the -CH_2- group is different. As we will show later, these differences affected the deposition quality of the films. We expect that this will also affect the rotational frequency of the -OH rotor and the formation/absence of tunneling phenomena as outlined by Alves *et. al.*[8].

3 Results

3a) Deposition of ω-F alkyne monolayers containing C_{18} carbon chains on Si 111 and Si 100 surfaces

In the first set of experiments for deposition of ω-F alkyne monolayers containing ten (C_{10}) and eighteen (C_{18}) carbon chains in their structure we followed the established literature protocols using an approach outlined by Pujari et.at.[6]. The C_{10} and C_{18} molecules were dissolved in toluene to form 50 mM and 100 mM dilutions. Then, they were deposited onto hydrogen terminated Si 111 surfaces for 1, 2 and 4 hours respectively. Mild heat of 80 °C was maintained. The surface analysis results are summarized in Table 1.

Table 1. Summary of experimental conditions and surface analysis of functionalizes Si 111. From the XPS analysis, concentrations of the carbon (C1s), fluorine (F1s), oxygen (O1s) and nitrogen (N1s) atoms are shown. WCA column shows for water contact angle measurements. R_q refers to average surface roughness obtained from atomic force microscopy analysis (AFM). In the composition of C_{10}^{*}, $C_{10}^{\#}$, $C_{18}^{\$}$ we found small amounts of chlor (Cl2p) and zinc (Zn2p) with combined concentration less than 2%.

SAM type	Dep. Time (hr)	Conc. (mM)	Chemical surface composition					WCA (°)	R_q (nm)
			C1s (at. %)	F1s (at. %)	O1s (at. %)	Si2p (at. %)	N1s (at. %)		
none			13.8	1.0	2.9	82.3	0	64	0.5±0.5
C_{10}^{*}	1	50	27.34	1.13	22.44	46.11	1.61	69	1.67±0.54
$C_{10}^{\#}$	2	50	35.1	1.48	22.17	38.11	2.19	68	1.23±0.07
$C_{18}^{\$}$	1	100	30.93	0.19	19.77	45.94	1.48	73	0.58±0.13
C_{18}	2	100	35	0.5	19.34	42.89	1.6	86	0.64±0.41
C_{18}	4	90	36.24	1.05	17.28	43.04	2.41	54	1.11±1.07

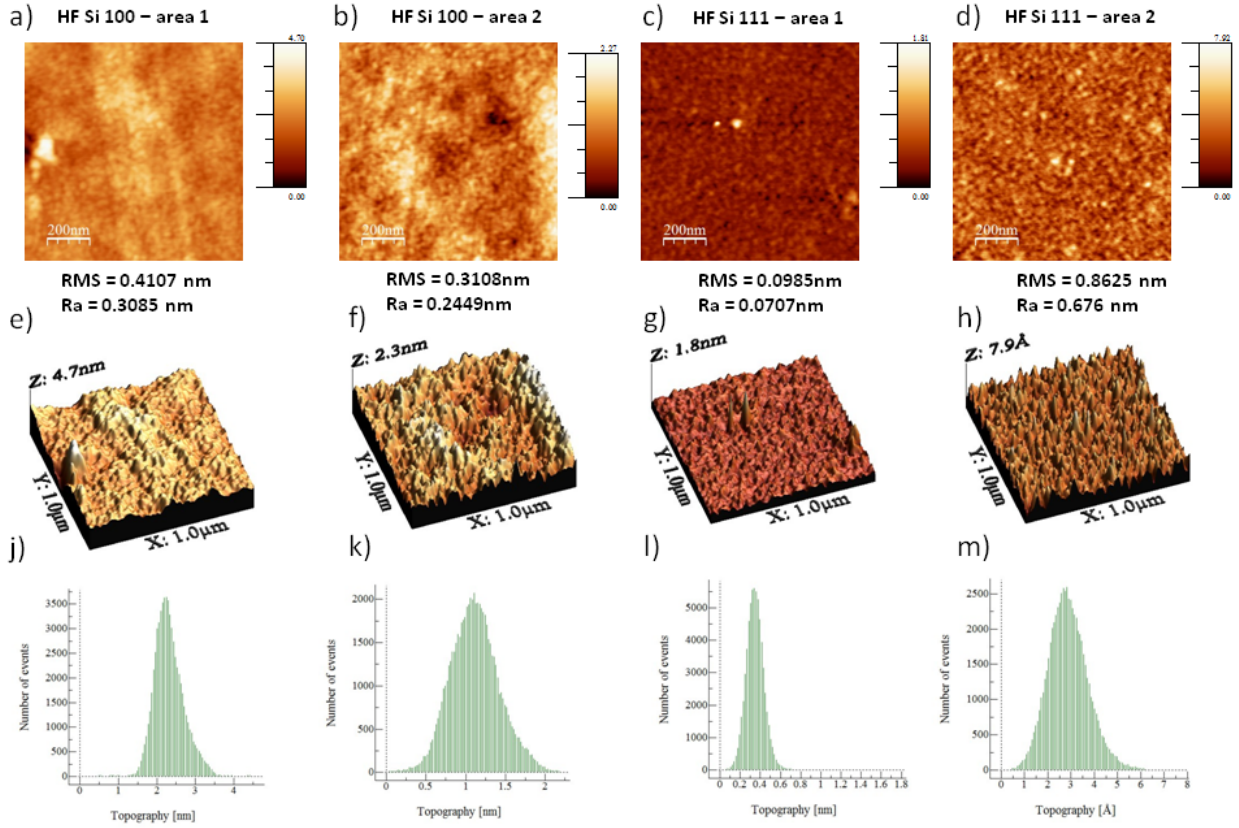

Figure 4. AFM analysis of couple areas of HF treated Si 100 and Si 111 surfaces. The topography of the first area is depicted in images a), e) and j) showing the 2D image (x, y direction); the 3D image and a histogram showing the analysis of the surface roughness respectively. Similar analyses were conducted for the other three areas. The surface roughness is shown under subfigures a), b), c) and d). An average of the RMS (R_q) roughness data are shown in Tables 1 and 3. The R_a is surface roughness calculated using different formula and is shown for completion.

Based on the results summarized in Table 1, we concluded that our preliminary deposition experiments were successful. Based on the molecular structure of fluorine SAMs, we expected increased amount of carbon (C1s concentration increased by 60 %). The fluorine concentration remained the same (due to only a CF group). The increased oxygen concentration in the SAM surfaces was due to adventitious carbon formed on the surface and formation of C-O, C=O and C-

O-N bonds. In the composition of C_{10}*, C_{10} #, $C_{18}$$ we found small amounts of chlor (Cl2p) and zinc (Zn2p) with combined concentration less than 2%.

Using the same functionalization approach, we exposed two hydrogen terminated TiN/Si chips to solutions of C_{18} and C_{10} self-assembled monolayers in toluene for one and two hours, respectively. Sections of the Si and the TiN areas from the chip surface were analyzed by XPS and the obtained results are summarized in Table 2. It should be pointed out that even though we denote the Si area from the TiN/Si chips, the XPS spot size was 400 μm and thus analysis encompassed both mostly Si and some of the TiN areas. Surprisingly, after two-hour deposition of C_{10}, the amount of incorporated fluorine doubled (1.5 to 3 at. %) for devices (Table 2) compared to H-Si surface (Table 1), while one-hour deposition of C_{18} increased the amount of incorporated fluorine by more than a factor of five to 1.7 at. %. This might be due to different affinity of molecule deposition due to Si crystal orientation - 111 (devices) vs. 100 (substrate only). Furthermore, we observed different deposition trends onto TiN films vs. Si surfaces, which is not surprising. However, overall our results demonstrated that SAMs were deposited onto TiN/Si devices.

Table 2. Summary of chemical surface analysis of functionalized TiN/Si devices by X-ray photoelectron spectroscopy (XPS).

SAM type	Dep. Time (hr)	Conc. (mM)	Device area	Chemical surface composition					
				C1s (at. %)	F1s (at. %)	O1s (at. %)	Si2p (at. %)	N1s (at. %)	Ti2p (at. %)
C_{10}	2	50	Si	42.42	3.16	24.15	8.8	10.52	8.83
C_{10}	2	50	TiN	43.22	1.93	26.02	0	14.32	12.87
C_{18}	1	50	Si	38.36	1.70	25.15	7.66	13.25	12.89
C_{18}	1	50	TiN	34.39	0.98	25.35	0	19.46	18.82

Even though these results were optimistic, we needed to verify that the SAMs coverage on the Si 111 surfaces was uniform. Note that in Table 1, in the case of C_{18} SAMs, the standard deviation in surface roughness especially after deposition for four hours was very large and the water contact angle was the smallest suggesting a surface with higher wettability. AFM analysis of multiple areas was performed before (Figure 4) and after (Figure 5) SAMs deposition. Several conclusions can be made from the images: 1) C_{10} covers the Si 111 surface differently than C_{18} which is easily understood as the molecule conformation and steric hindrance of the molecular chains is different; 2) the shortest deposition time of one hour produced the best results due to smaller agglomeration (note the large agglomerates after two- and four- hours depositions). We also could not reproduce the water contact angles of 94° and 110° for C_{10} and C_{18} SAMs cited in the literature, respectively. We achieved 69° and 73° for C_{10} and C_{18} SAMs respectively, which is close to the values of Sieval *et.al.*[5] for C_{10} SAMs of 77°.

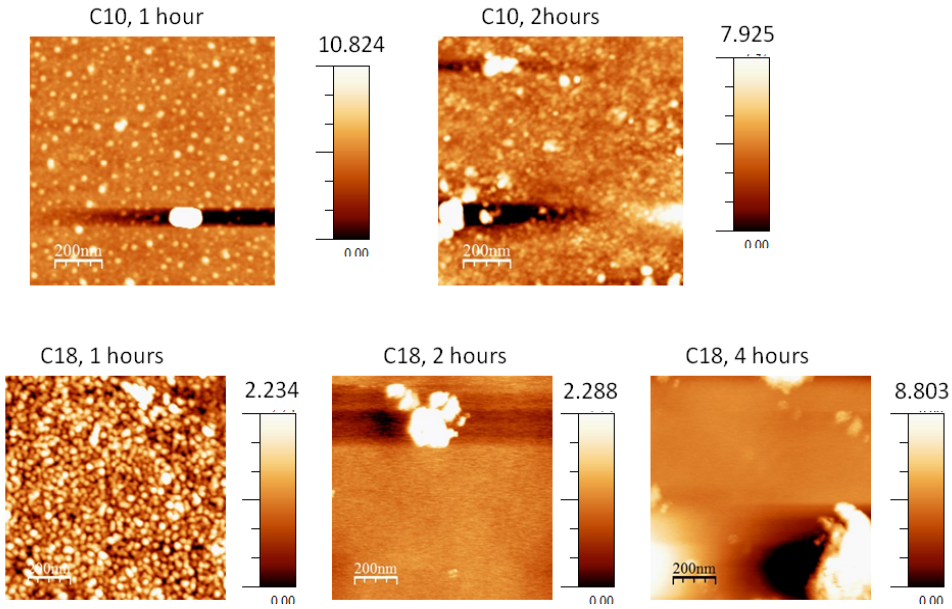

Figure 5. Atomic force microscopy images of ω-F alkyne monolayers with C_{10} and C_{18} carbon chains. The 2D images show x and y direction of the scan, the z-scale is shown on the right side of each image.

We hypothesized that the density of formation of the Si-C bonds was not efficient enough. Several parameters could be used to increase deposition efficiency and foster formation of Si-C bonds – SAMs powder concentration in solvent (solution molarity), temperature, solvent type, and incorporation of catalyst. The deposition process could also be affected by the type of Si substrate – this has been observed in many applications such as gold nanoparticles deposition, and growth of superconducting materials on Si substrate. The deposition temperature was indirectly affected by the type of the organic solvent used as we needed to prevent solvent evaporation. For example, in case of toluene with boiling temperature of 110 °C, a safe SAMs deposition occurred at temperatures < 90 °C. Thus, choosing an inorganic solvent with higher boiling temperature might enable better mixing and different deposition efficiency.

For the next experimental set, we focused on ω-F alkyne monolayers with C_{18} carbon chains deposition. We investigated the effects of SAMs powder concentration in solvent (solution molarity), catalyst, heating and crystal orientation of Si substrates. We kept the solvent (toluene) and the deposition time the same. The exact experimental conditions are depicted in Table 3. Figures 6-11 show the morphology analysis of multiple areas for each experimental condition.

Table 3. Summary of experimental conditions and surface analysis of functionalizes Si 111 and Si 100 surfaces. WCA column shows for water contact angle measurements. R_q refers to average surface roughness obtained from AFM, WCA denotes a water contact angle. Note that Si 111 and Si 100 surfaces were hydrogen terminated using 49 % HF, for 2 minutes at room temperature prior SAMs deposition.

Substrate	SAMs	Conc. (mM)	Temp. (°)	Dep. Time (hr)	solvent	catalyst	WCA (°)	R_q (nm)
Si 111						no	64	0.50 ± 0.5
Si 100						no	75	0.27 ± 0.1
Si 111	C_{18}	50	25	24	toluene	yes	65	3.56 ± 3.6
Si 111	C_{18}	50	80	24	toluene	yes	65	1.73 ± 0.7
Si 111	C_{18}	100	25	24	toluene	yes	79	1.74 ± 0.8
Si 111	C_{18}	100	80	24	toluene	yes	77	0.38 ± 0.1
Si 100	C_{18}	100	80	24	toluene	yes	72	1.15 ± 1.0
Si 100	C_{18}	50	80	24	toluene	yes	74	1.73 ± 0.7

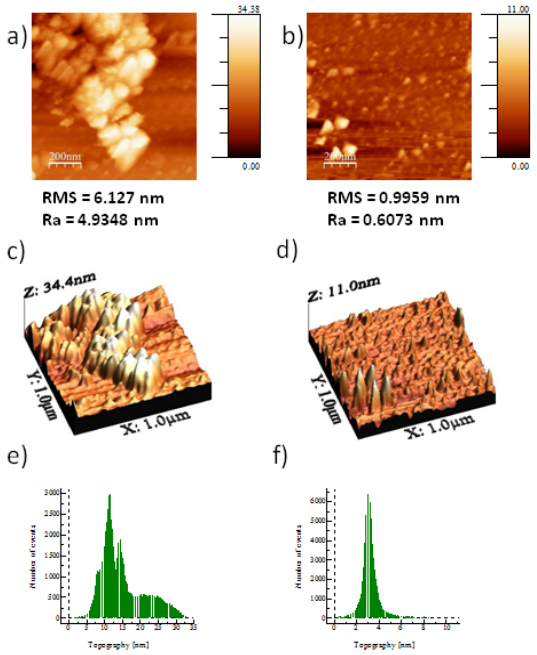

Figure 6. AFM analysis of two areas of Si 111 surface coated with ω-F alkyne SAMs with C_{18} carbon chains. SAMs are deposited in 50 mM concentration in toluene at room temperature with Pt catalyst. The topography of the first area is depicted in images a), c) and e) showing the 2D image (x,y direction); the 3D image and a histogram showing the analysis of the surface roughness respectively. Similar analyses were conducted for the second area and the data is depicted in subfigures b), d) and f) respectively. The surface roughness is shown under subfigures a) and b). An average of the RMS (R_q) roughnesses is shown in Table 3. The R_a is surface roughness calculated using different formula and is shown for completion.

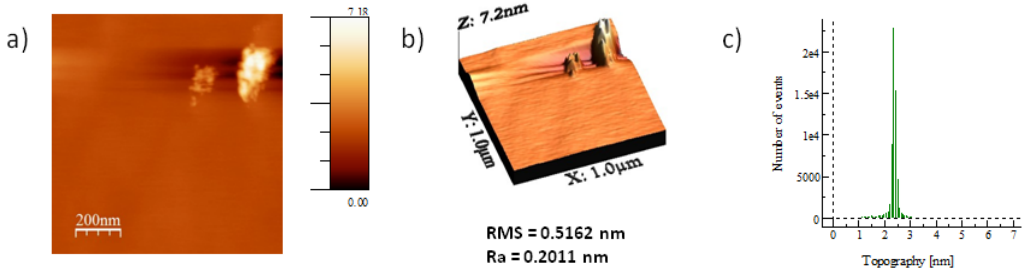

Figure 7. AFM analysis of two areas of Si 111 surface coated with ω-F alkyne SAMs with C_{18} carbon chains. SAMs are deposited in 50 mM concentration in toluene at 80 °C with Pt catalyst. The topography is depicted in images a), b) and c) showing the 2D image (x, y direction); the 3D image and a histogram showing the analysis of the surface roughness respectively. The surface roughness is shown under subfigure b). The R_a is surface roughness calculated using different formula and is shown for completion.

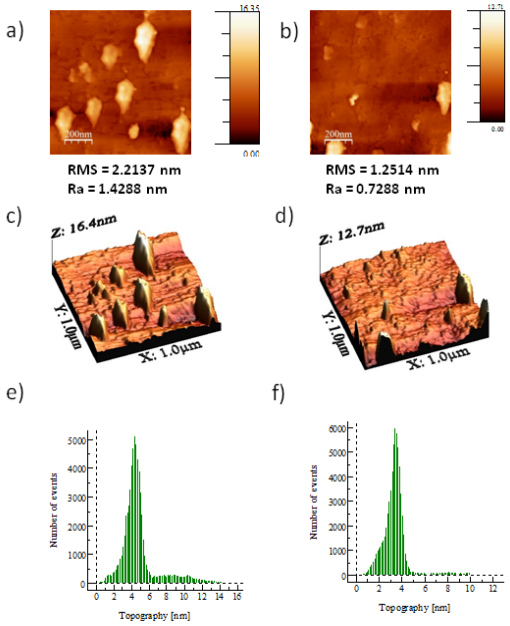

Figure 8. AFM analysis of two areas of Si 100 surface coated with ω-F alkyne SAMs with C_{18} carbon chains. SAMs are deposited in 50 mM concentration in toluene at 80 °C with Pt catalyst. The topography of the first area is depicted in images a), c) and e) showing the 2D image (x, y direction); the 3D image and a histogram showing the analysis of the surface roughness respectively. Similar analysis was conducted for the second area and the data is depicted in subfigures b), d) and f) respectively. The surface roughness is shown under subfigures a) and b). An average of the RMS (R_q) roughnesses is shown in Table 3. The R_a is surface roughness calculated using different formula and is shown for completion.

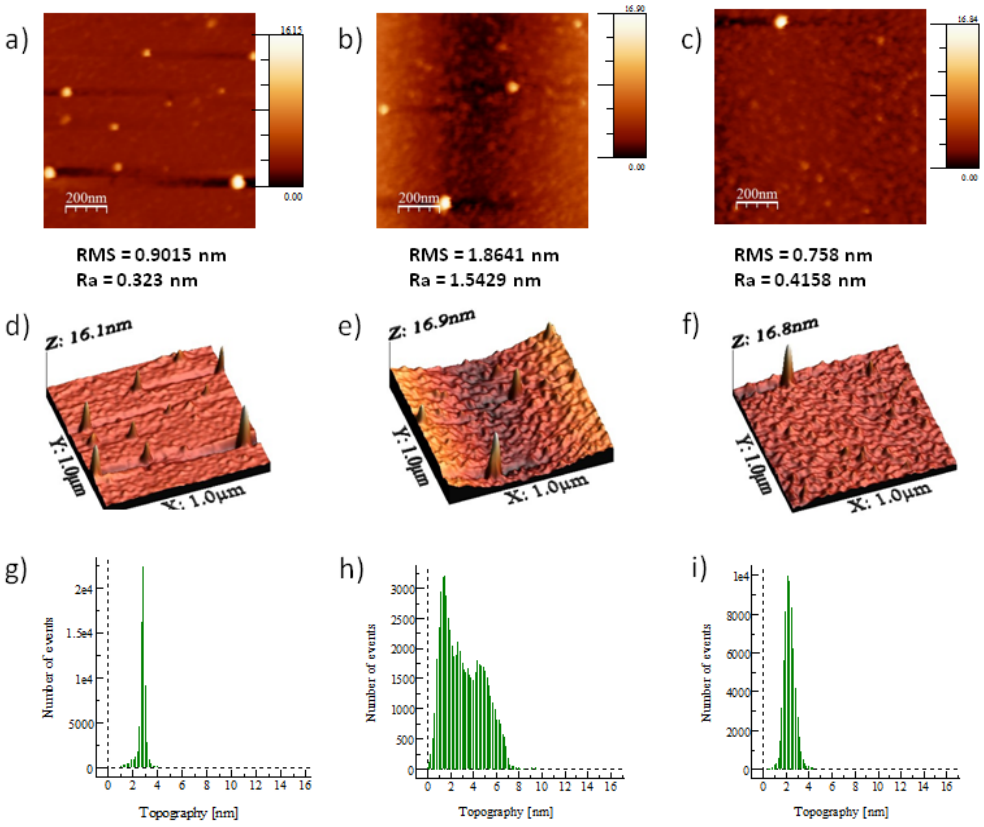

Figure 9. AFM analysis of three areas of Si 111 surface coated with ω-F alkyne SAMs with C_{18} carbon chains. SAMs are deposited in 100 mM concentration in toluene at room temperature with a Pt catalyst. The topography of the first area is depicted in images a), d) and g) showing the 2D image (x, y direction); the 3D image and a histogram showing the analysis of the surface roughness, respectively. Similar analysis was conducted for the other two areas and the data is depicted in subfigures b), e) and h) for the second area and c), f) and I) for the third area, respectively. The surface roughness is shown under subfigures a), b) and c). An average of the RMS (R_q) roughnesses is shown in Table 3. The R_a is surface roughness calculated using different formula and is shown for completion.

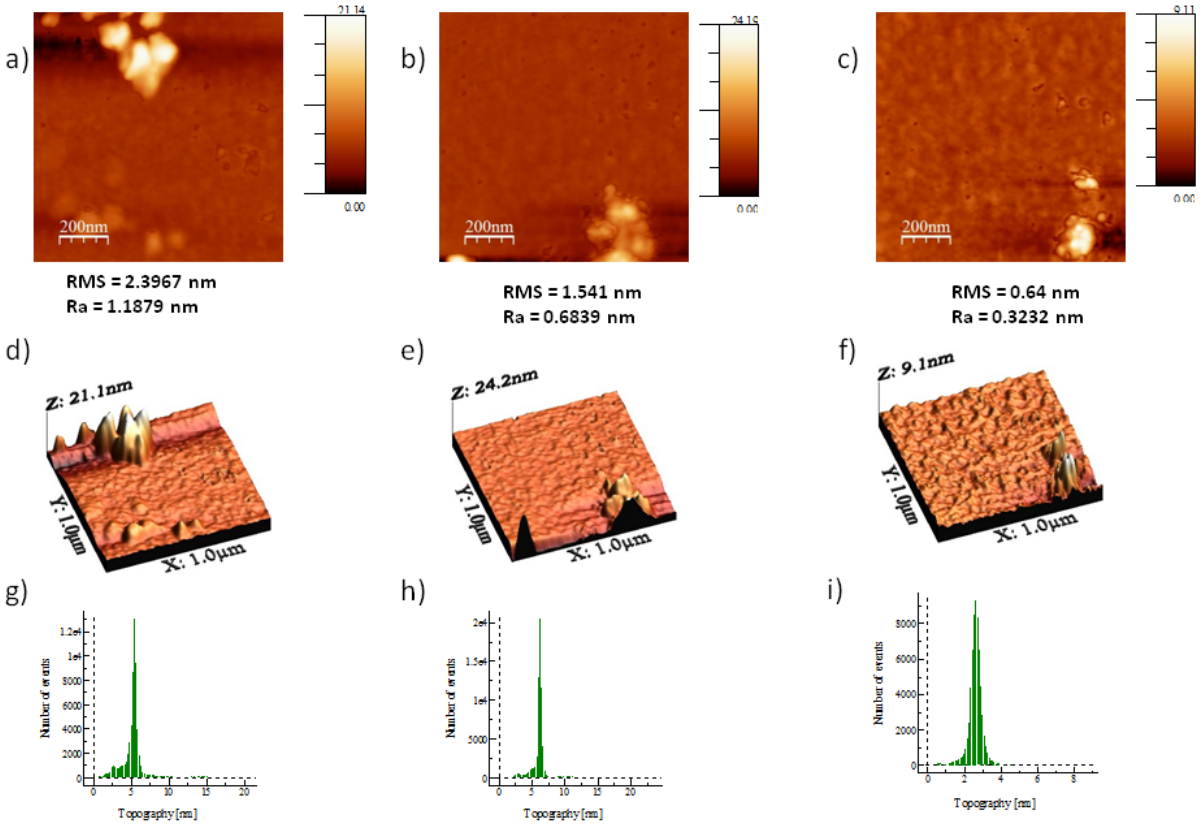

Figure 10. AFM analysis of three areas of Si 111 surface coated with ω-F alkyne SAMs with C_{18} carbon chains. SAMs are deposited in 100 mM concentration in toluene at 80 °C with Pt catalyst. The topography of the first area is depicted in images a), d) and g) showing the 2D image (x,y direction); the 3D image and a histogram showing the analysis of the surface roughness, respectively. Similar analysis was conducted for the other two areas and the data is depicted in subfigures b), e) and h) for the second area and c), f) and I) for the third area, respectively. The surface roughness is shown under subfigures a), b) and c). An average of the RMS (R_q) roughnesses is shown in Table 3. The R_a is surface roughness calculated using different formula and is shown for completion.

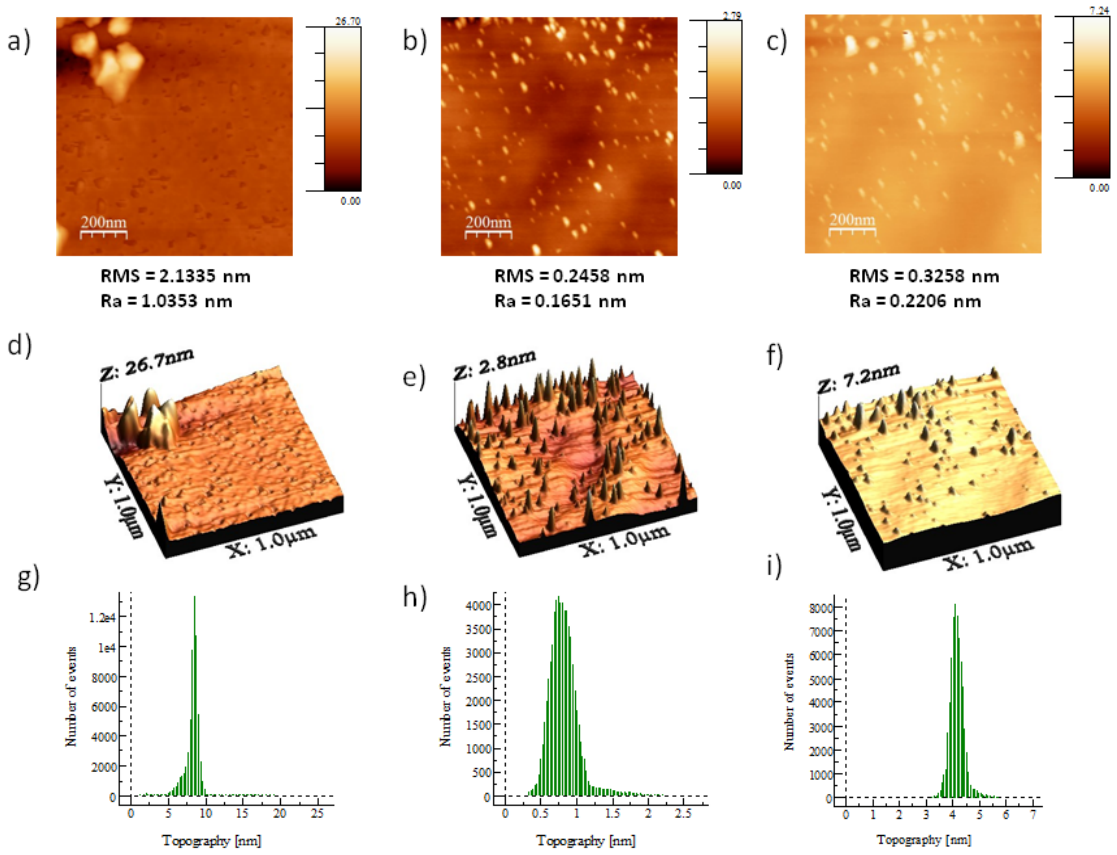

Figure 11. AFM analysis of two areas of Si 100 surface coated with ω-F alkyne SAMs with C_{18} carbon chains. SAMs are deposited in 100 mM concentration in toluene at 80 °C with a Pt catalyst. The topography of the first area is depicted in images a), c) and e) showing the 2D image (x, y direction); the 3D image and a histogram showing the analysis of the surface roughness, respectively. Similar analyses were conducted for the second area and the data is depicted in subfigures b), d) and f), respectively. The surface roughness is shown under subfigures a) and b). An average of the RMS (R_q) roughnesses is shown in Table 3. The R_a is surface roughness calculated using different formula and is shown for completion.

Deposition of ω-F alkyne SAMs with C_{18} carbon chains on Si 111 and Si 100 surfaces was challenging. Our goal was to achieve smooth films (R_q< 0.5 nm), high water contact angle (WCA > 100 °), and high carbon C1s and F1s values. Even though the deposition was dependent on the number of carbon atoms in a chain (C_{10} vs. C_{18}) and Si crystal orientation (Si 111 vs. Si 100) some general trends emerged. SAM deposition in higher temperature was more favorable and solution molarity did not have significant effect to the chemical composition of the resulting SAM films. The SAMs films uniformity was affected by the presence of catalyst during deposition, producing overall smoother films. For the best deposition of C_{18} molecules on Si 111 surface WCA was almost 80° and the AFM analysis showed smooth surface (R_q< 0.5 nm). Chemically, at these deposition conditions we detected the highest carbon concentration of 40 at. %, halving of the concentration of Si and O1s compared to the untreated Si substrates (Figure 12, Table 4). Small amount of fluorine was detected as well (< 1%). In addition, our XPS results suggested that the SAMs were oriented in the correct way – with Si-C bond formed between Si surfaces and the SAM and the CF group pointing away from the surface (Figure 13).

Table 4. Chemical composition of the ω-F alkyne SAMs with C_{18} carbon chains on Si 111 and Si 100 surfaces

Substr -ate	**SAM**	**Conc. (mM)**	**Temp. (°C)**	**Chemical composition analysis**				
				C1s (at. %)	O1s (at. %)	Si2p (at. %)	F1s (at. %)	Pt4f (at. %)
Si 111		49%	25	16.5 ± 4	9 ± 0.5	73.4 ± 1.7	0	0
Si 100		49%	25	16.6 ± 1.4	9 ± 0.4	74.4 ± 1.8	0	0
Si 111	C_{18}	50 mM	25	30.9 ± 1.1	24.2 ± 0.4	42.9 ± 0.8	0	0.3±0.02
Si 111	C_{18}	50 mM	80	39.6 ± 0.3	20.6 ± 0.1	37.1 ± 0.5	0.5 ± 0.1	0.3±0.03
Si 111	C_{18}	100 mM	25	35.9 ± 1.4	21.9 ± 0.7	40 ± 1	0.48	0.3±0.01
Si 111	C_{18}	100 mM	80	40.2 ± 0.4	20.3 ± 0.6	37.8 ± 0.4	0.3 ± 0.1	0.5±0.03
Si 100	C_{18}	100 mM	80	37.8 ± 0.4	21 ± 0.3	37.9 ± 0.7	0.6 ± 0.04	0.3
Si 100	C_{18}	50 mM	80	37.3 ± 1.7	20 ± 0.1	40.8 ± 0.8	0.8 ± 0.04	0.38

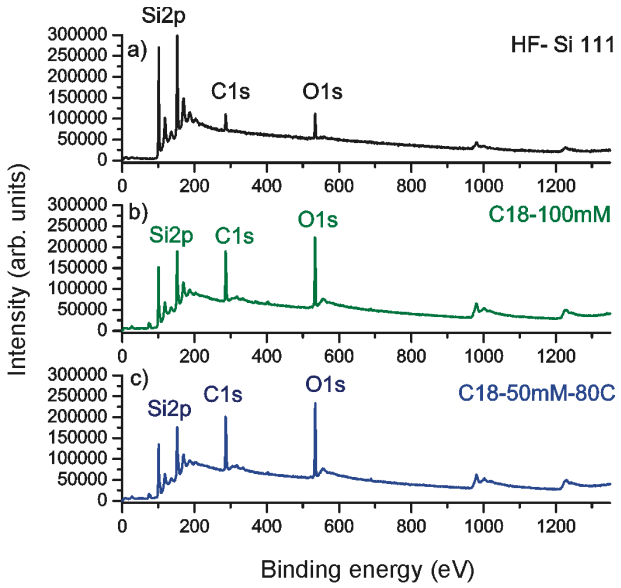

Figure 12. Survey spectra of ω-F alkyne SAMs with C_{18} carbon chains on Si 111 surface under optimal conditions: 50 mM concentration of C18 in toluene at 80 °C for 24 hours deposition time (b) and 100 mM concentration of C_{18} in toluene at room temperature for 24 hours deposition time (c). The composition of HF – treated Si (a) is shown for comparison.

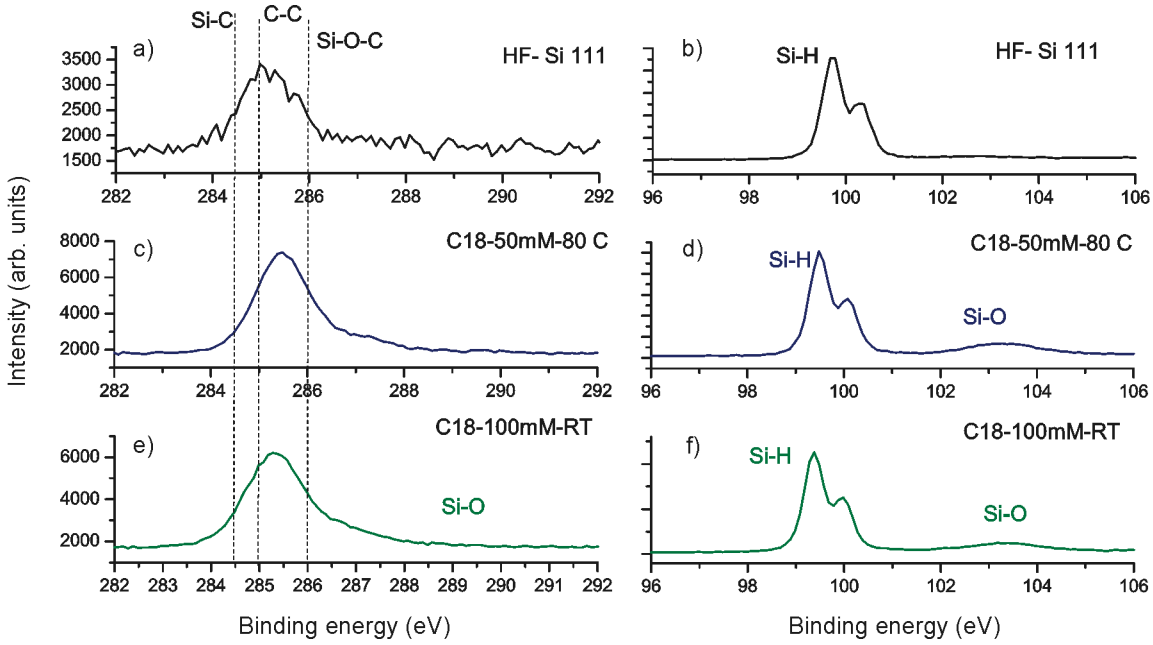

Figure 13. High resolution C1s and Si2p regions of ω-F alkyne SAMs with C_{18} carbon chains on Si 111 surface under optimal conditions: 50 mM concentration of C18 in toluene at 80 °C for 24 hours deposition time (c, d) and 100 mM concentration of C_{18} in toluene at room temperature for 24 hours deposition time.

Summary for deposition of ω-F alkyne SAMs with C_{10} and C_{18} carbon chains on Si

Deposition of ω-F alkyne SAMs with C_{10} and C_{18} carbon chains on Si was challenging. Established literature protocols did not produce closely packed monolayers with superhydrophobic nature (WCA > 100 °). We demonstrated a viable deposition path and identified two key deposition parameters: high temperature (T > 80 °C) and presence of catalyst during deposition. We also observed that molarity concentration of molecular solutions was not as important as the Si crystal orientation. Further experiments are needed to further optimize the deposition process. We believe that change the solvent from toluene to 1-hexadecane, would allow for higher deposition temperature of 110 °C compared to currently used 80 °C. This would ideally form a relatively thick monolayer of 2 nm, with water contact angle of 110° and no agglomeration fragments.

3b) Deposition of VP, EP, and VPM on hydrogen terminated Si 111 and Si 100 surfaces

The deposition of VP, EP, and VPM were conducted in a similar fashion as the of ω-F alkyne SAMs with C_{10} and C_{18} carbon chains. Table 5 summarizes the deposition details. Briefly, Si 111 surfaces were treated in 49 % hydrofluoric acid (HF) for 2 minutes to remove the native SiO_2 layer. VPM, EP, VP were dissolved in toluene and 50 mM and 100 mM solutions were prepared. These solutions were deposited onto Si 111 surfaces at room temperature and at 80 °C in the presence of Pt catalyst. Great care was taken to dry the glassware before SAMs deposition as the presence of oxygen was limiting the deposition reaction. The VPM, EP, VP molecules had very similar composition containing CH_2 functional group, benzene ring and -OH functionality as shown in Figure 3. The difference between VPM and EP phenol was that -OH was present as -CH_2OH functionality in VPM, and was attached directly to the benzene ring in EP. The difference

between EP and VP was the relative position between -OH and -CH_2- functionalities (3- vs. 4-). As we show below, these small differences affected the deposition process. Table 5 shows water contact angle measurements, X-ray photoelectron spectroscopy and atomic force microscopy analysis of surface energy and composition, as well as surface morphology of deposited SAMs on Si 111 and Si 100 substrates. Multiple areas on each sample were analyzed.

Table 5. Summary of experimental conditions and surface analysis of deposition of VP, EP, and VPM on Si 111 and Si 100 surfaces. WCA column shows for water contact angle measurements. HF denotes hydrofluoric acid.

Substrate	SAMs	Conc. (mM)	Temp. (°C)	Dep. Time (hr)	Solvent	Catalyst	WCA (°)
Si 111						no	64
Si 100						no	75
Si 111	EP	50	25	24	toluene	yes	70
Si 111	EP	100	25	24	toluene	yes	80
Si 111	EP	50	80	24	toluene	yes	83
Si 111	EP	100	80	21	toluene	yes	76
Si 111	VP	50	25	24	toluene	yes	62
Si 111	VP	100	25	24	toluene	yes	55
Si 111	VP	50	80	24	toluene	yes	59
Si 111	VP	100	80	21	toluene	yes	61
Si 111	VPM	50	25	24	toluene	yes	56
Si 111	VPM	100	25	24	toluene	yes	72
Si 111	VPM	50	80	24	toluene	yes	70
Si 100	EP	50	80	24	toluene	yes	90
Si 100	EP	100	80	21	toluene	yes	73
Si 100	VP	50	80	24	toluene	yes	68
Si 100	VP	100	80	21	toluene	yes	58

We expected that deposition of EP, VP, and VPM molecules on Si 111 and Si100 would increase the water contact angle (produce a more hydrophobic surface) as the amount of oxygen (OH)

contained in each molecule was limited. Thus, we could use the WCA as a measure of molecular surface coverage. Consistent with the SAMs deposition, the WCA indeed increased with the highest detected WCA increase of 90 ° for EP deposition at high temperature of 80 °C. Note that these depositions were conducted only with the presence of catalyst for prolonged deposition time (>20 hours). The best deposition concentration on Si 111 for EP and VPM was 50 mM, while for VP was 100 mM. VP and EP, at high temperature, were deposited on Si 100 surface and the best deposition was achieved with 50 mM solution concentration in toluene (Table 5).

As shown in Figure 14 and Figure 15, as well as in Table 6, the chemical composition of VP, EP and VPM deposition on Si surfaces correlated well with the WCA measurements. The C1s concentration and thus the thickness of the molecular layer increased in the following order VP, VPM and EP respectively. The smallest amount of O1s and Si2p of 22 % and 13 % respectively, were detected in the EP case as well. This might be due to EP polymerization and thus multilayer formation. The amount of detected catalyst was also more than a factor of five higher compared to the VP and VPM molecules.

Figure 16 and Figure 17 show the high-resolution Si 2p and C1s regions spectra and provide further information about the nature of the chemical environment for each molecule on Si surface. The Si region showed formation of the Si-O bonds for VP, EP and VPM. For EP we observed that formation of C-O-Si dominated the Si-O bond formation. The presence of Si-C bonds was confirmed from the analysis of the C1s regions as well for the VP, EP and VPM attachment to both Si 111 and Si 100 surfaces. Formation of C-C and C-OH bonds confirmed the presence of the organic molecular layers on the Si surfaces as well.

Table 6. Chemical composition of the EP, VP and VPM on Si 111 and Si100 surfaces

Substrate	SAMs	Conc. (mM)	Temp. (°C)	Chemical composition of Si surface			
				C1s (at. %)	O1s (at. %)	Si2p (at. %)	Pt4f 9at. %)
Si111				17 ± 4.0	9 ± 0.50	73 ± 1.7	0
Si 100				17 ± 1.4	9 ± 0.40	74 ± 1.8	0
Si111	EP	50	25	31 ± 0.6	27 ±0.01	41 ± 0.6	0.5 ± 0.01
Si111	EP	100	25	26 ± 0.4	27 ±1.60	47 ± 0.2	0.7 ± 0.01
Si111	EP	50	80	55 ± 0.7	22 ± 0.40	14 ± 0.1	5.0 ± 0.01
Si111	EP	100	80	53 ± 0.5	22 ± 0.20	8 ± 0.1	10.0 ± 0.30
Si111	VP	50	25	22 ± 3.4	25 ± 0.80	52 ± 2.8	0.4 ± 0.02
Si111	VP	100	25	27 ± 1.1	22 ± 1.7	50 ± 1.8	0.3 ± 0.00
Si111	VP	50	80	19 ± 2.8	31 ± 2.5	50 ± 1.3	0.1 ± 0.01
Si111	VP	100	80	30 ± 4.3	29 ± 0.2	41 ± 5.0	0.2 ± 0.03
Si111	VPM	50	25	19 ± 0.2	23 ± 0.7	50 ± 1.8	0.3 ± 0.00
Si111	VPM	100	25	27 ± 3.1	23 ± 1.0	48 ± 2.9	0.3 ± 0.04
Si 111	VPM	50	80	31 ± 0.2	24 ± 0.1	44 ± 0.1	0.3 ± 0.01
Si100	EP	50	80	53 ± 0.7	23 ± 0.10	14 ± 1.2	6 ± 0.30
Si100	EP	100	80	48 ± 3.1	20 ± 0.04	16 ± 0.4	9 ± 0.20
Si100	VP	50	80	25 ± 3.6	32 ± 0.20	43 ± 2.4	0.5 ± 0.01
Si100	VP	100	80	19 ± 1.2	30 ± 1.20	51 ± 1.1	0.3 ± 0.11

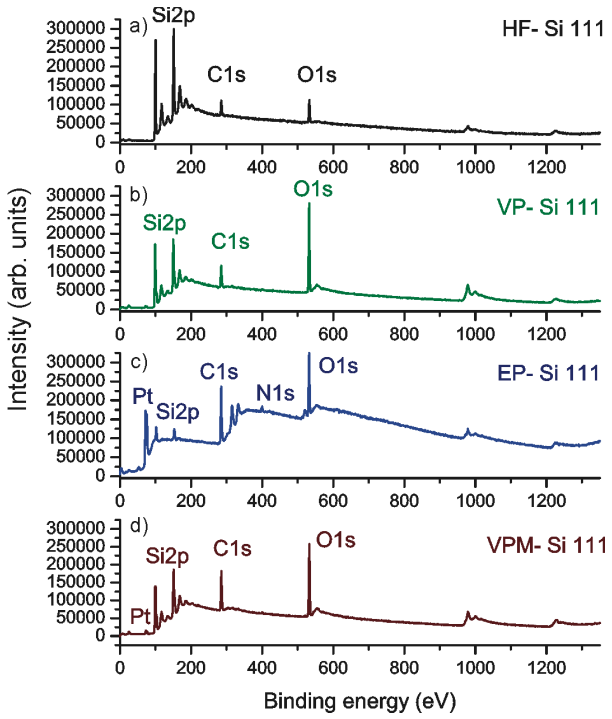

Figure 14. Survey spectra of VP, EP, and VPM on Si 111 and Si 100 surfaces under optimal deposition conditions: concentration of 100 mM at 80 °C for VP (b), concentration of 50 mM at 80 °C for EP (c), concentration of 50 mM at 80 °C for VPM (d). The survey of HF-treated Si 111 surface (a) is shown for comparison.

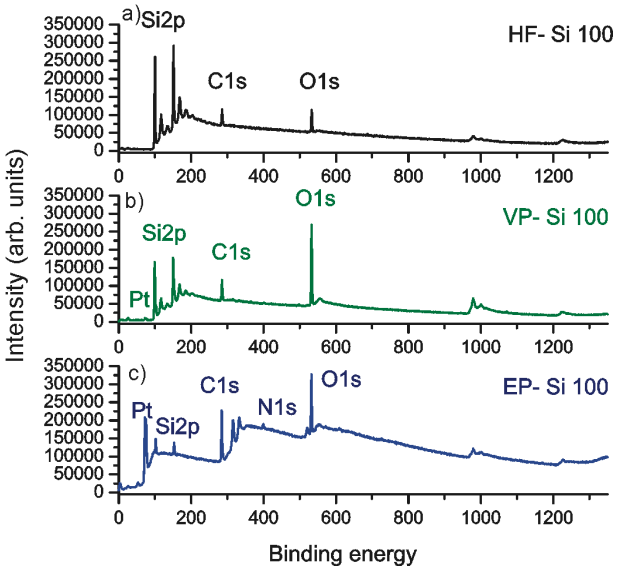

Figure 15. Survey spectra of VP and EP (c) and on Si 100 surfaces at best deposition conditions: concentration of 50 mM at 80 °C. The survey of HF-treated Si 100 surface (a) is shown for comparison.

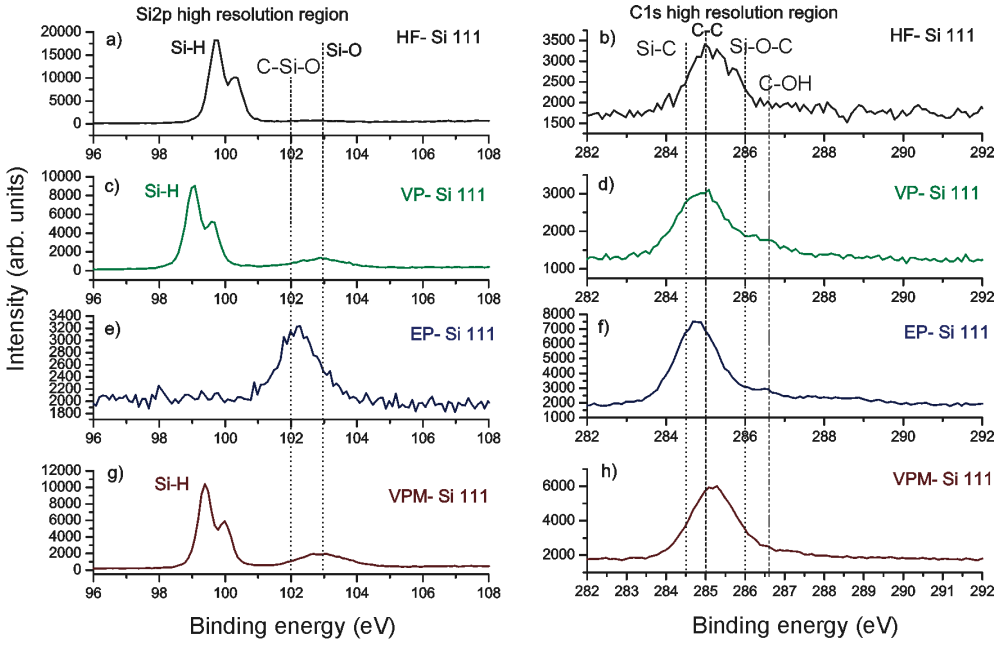

Figure 16. High resolution Si 2p and C1s spectra of VP, EP, and VPM on Si 111 under optimal deposition conditions: concentration of 100 mM at 80 °C for VP (c, d), concentration of 50 mM at 80 °C for EP (e, f), concentration of 50 mM at 80 °C for VPM (g, h). The high-resolution Si 2p and C1s spectra of HF-treated Si 111 surface (a, b) is shown for comparison.

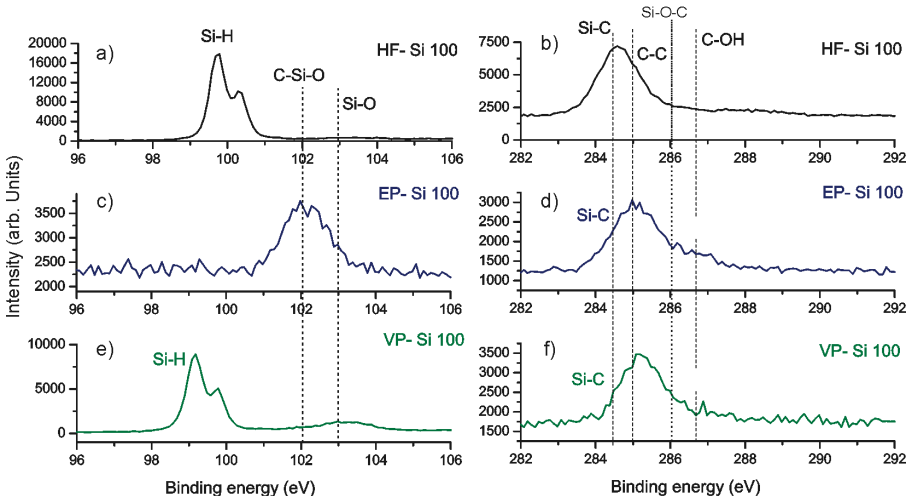

Figure 17. High-resolution Si 2p and C1s spectra of EP (c, d) and VP (e, f) on Si 111 under optimal deposition conditions: concentration of 50 mM at 80 °C. The high-resolution Si 2p and C1s spectra of HF-treated Si 100 surface (a, b) are shown for comparison.

Table 7 summarizes the surface roughness values for EP, VP and VPM molecular films deposited on Si111 and Si100 surfaces. While Figure 18 shows the morphology of selected areas of EP, VP and VPM molecules deposition on Si 111 is shown in, Figure 19 shows the morphology of the EP and VP molecular films deposited on Si 100 surfaces. In general, EP produced films with higher roughness most likely due to thicker polymerized films unrelated to Si crystal orientation. For VP, solution concentration had a greater impact on film roughness than deposition temperature. The highest roughness value was comparable to the EP rough films for Si111 surfaces. Deposition on Si 100 surfaces produced rough films for both VP and EP molecules with R_q (EP> R_q (VP). VPM molecules produced the smoothest films – in general the R_q reduction was more than a factor of two compared to the reference H-Si surface.

Table 7. Summary of surface roughness obtained from AFM of functionalizes Si 111 and Si 100 surfaces. R_q refers to the average (RMS) surface roughness

Substrate	SAMs	Conc. (mM)	Temp. (°)	Dep. Time (hr)	R_q (nm)
Si 111					0.5 ± 0.5
Si 111	VP	50	25	24	0.3 ± 0.1
Si 111	VP	100	25	24	0.9 ± 0.3
Si 111	VPM	50	25	24	0.2 ± 0.1
Si 111	VPM	100	25	24	0.5 ± 0.4
Si 111	EP	50	80	24	1.5 ± 0.5
Si 111	VP	100	80	21	1. ± 0.5
Si 111	VPM	100	80	24	0.134
Si 100					0.3 ± 0.4
Si 100*	EP	50	80	24	3.5 ± 3.5
Si 100	VP	50	80	24	2.2 ± 0.1

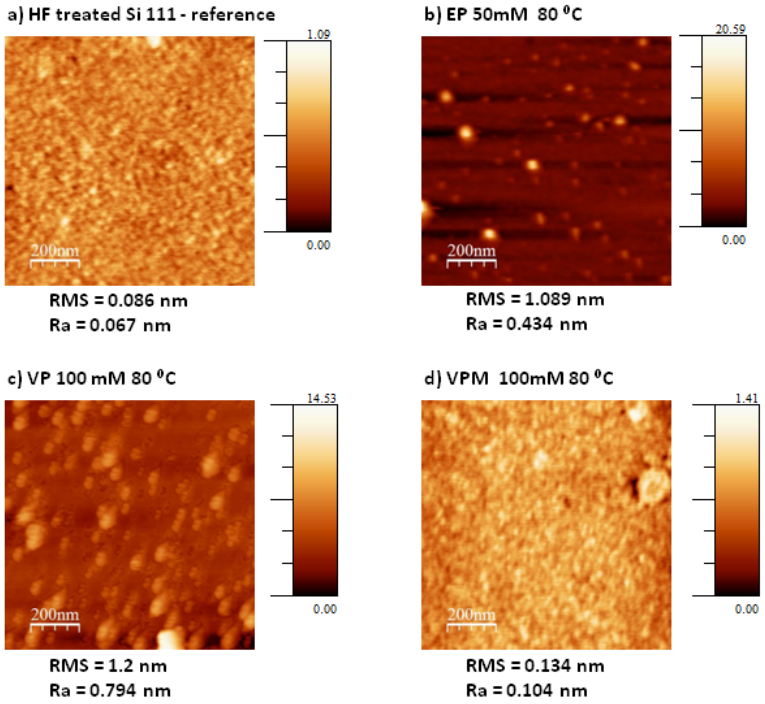

Figure 18. Changes of surface morphology based on AFM analysis due to deposition of VP, EP, and VPM (d) on Si 111 surfaces. HF treated Si 111 surface (a) is shown as reference. The surface roughness is shown under each subfigure. An average of the RMS (R_q) roughnesses is shown in Table 7. The R_a is surface roughness calculated using different formula and is shown for completion.

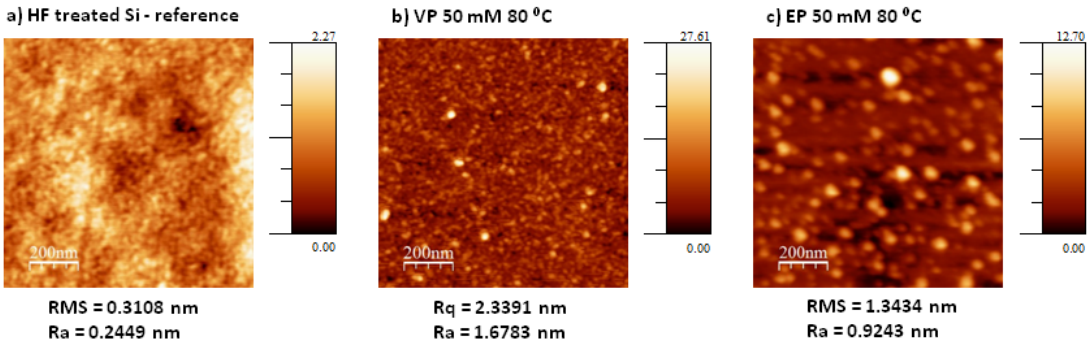

Figure 19. Changes of surface morphology based on AFM analysis due to deposition of VP (b) and EP (c) on Si 111 surfaces. HF treated Si 100 surface (a) is shown as reference. The surface roughness is shown under each subfigure. An average of the RMS (R_q) roughnesses is shown in Table 7. The R_a is surface roughness calculated using different formula and is shown for completion.

Summary for deposition of VP, EP, and VPM on Si 111 and Si 100 surfaces

The protocols developed for deposition of VP, EP, and VPM on hydrogen terminated Si 111 and Si 100 surfaces were completely novel. We believe that we achieved a multilayer of EP as signified by production of hydrophobic surface with significantly modified surface elemental composition and high surface roughness. Successful deposition of VPM and VP molecules was demonstrated as well. Even though further experiments are needed to optimize the deposition process, we believe that increasing the deposition temperature while keeping a low molecular concentration of 50 mM solutions will yield the desired densely packed molecular surfaces.

4. Overall summary and future work

Identifying the sources of loss in dielectric materials, and understanding their influence onto the superconducting microwave resonator performance is a critical step for the advancement of quantum technology. In this work, we developed novel synthesis approaches and deposition protocols of chemical molecular films with artificial molecular rotors (OH-, and CF- groups) in their structure. This is a novel research area for both superconducting quantum computing and chemical surface sciences. Even though we showed successful deposition of C_{10}, C_{18}, EP, VP, and VPM molecules, further experiments are needed, namely at increased deposition temperatures and in the presence of a catalyst. We believe that a concentrated research effort on understanding the effects of molecular rotors on microwave resonator performance may lead to a better fundamental understanding of the nature of the loss in dielectric materials which may in turn enable development of strategies for increasing Q_is.

Appendix

Examples of AFM surface area analysis of VPM, EP and VP molecules on Si 111 and Si100 surfaces

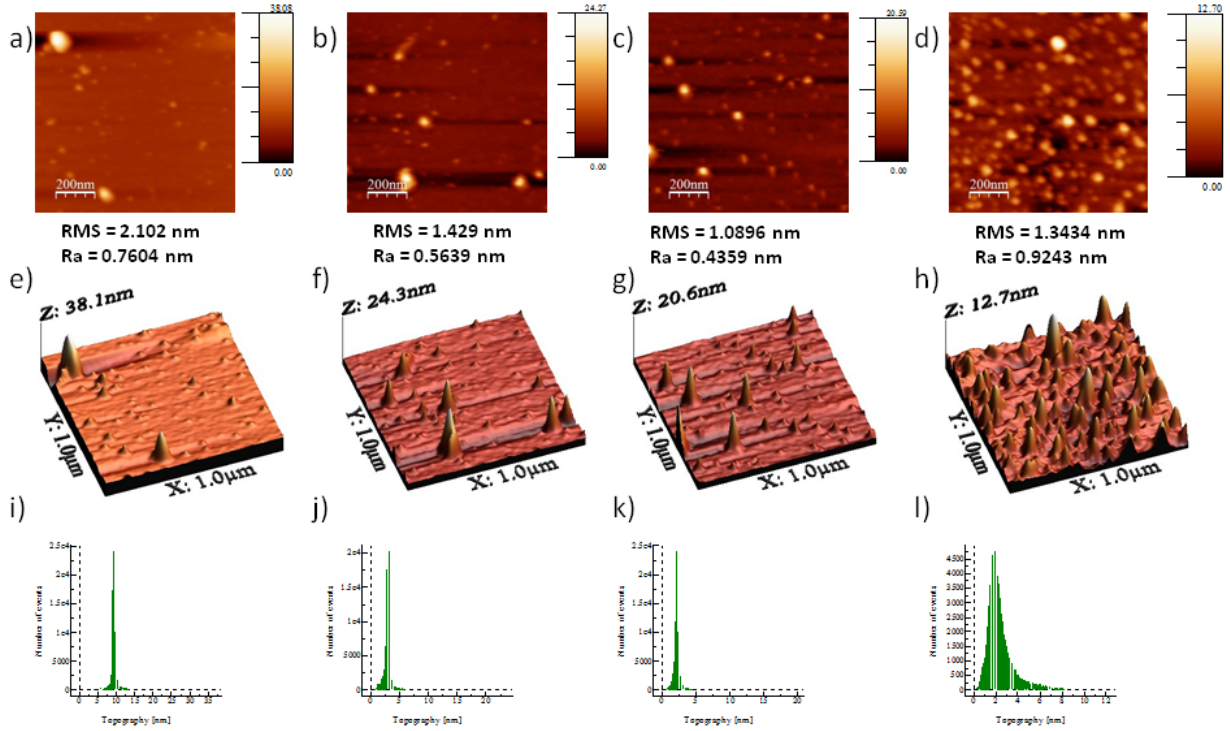

Figure A1. AFM analysis of four areas of Si 111 surface coated with 50 mM concentrated solution of EP in toluene at 80 °C with Pt catalyst. The topography of the first area is depicted in images a), e) and j) showing the 2D image (x, y direction); the 3D image and a histogram based on which the surface roughness was estimated. Similar analysis was conducted for all areas. The surface roughness is shown under subfigures a), b), c) and d). An average of the RMS (R_q) roughnesses is shown in Table 5. The R_a is surface roughness calculated using different formula and is shown for completion.

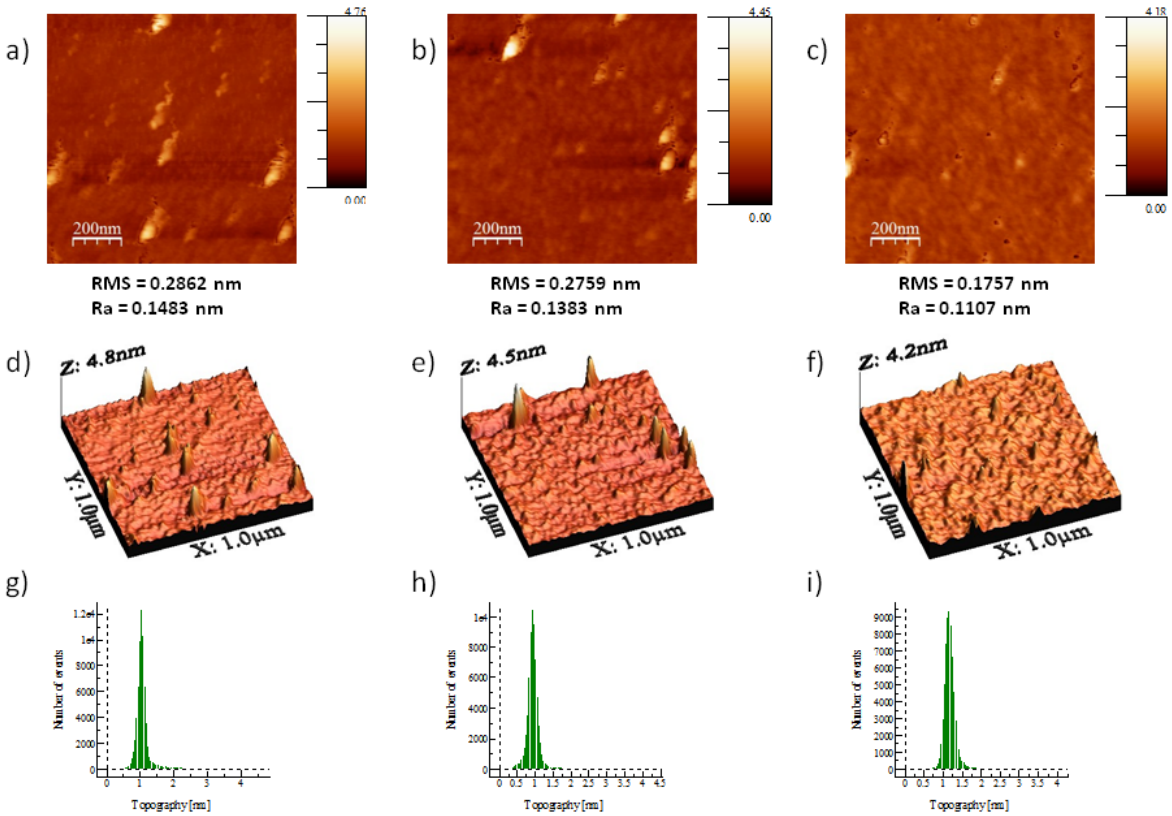

Figure A2. AFM analysis of three areas of Si 111 surface coated with 50 mM concentrated solution of VP in toluene at 80 °C with Pt catalyst. The topography of the first area is depicted in images a), d) and g) showing the 2D image (x, y direction); the 3D image and a histogram based on which the surface roughness was estimated. Similar analysis was conducted for all areas. The surface roughness is shown under subfigures a), b), and c). An average of the RMS (R_q) roughnesses is shown in Table 5. The R_a is surface roughness calculated using different formula and is shown for completion.

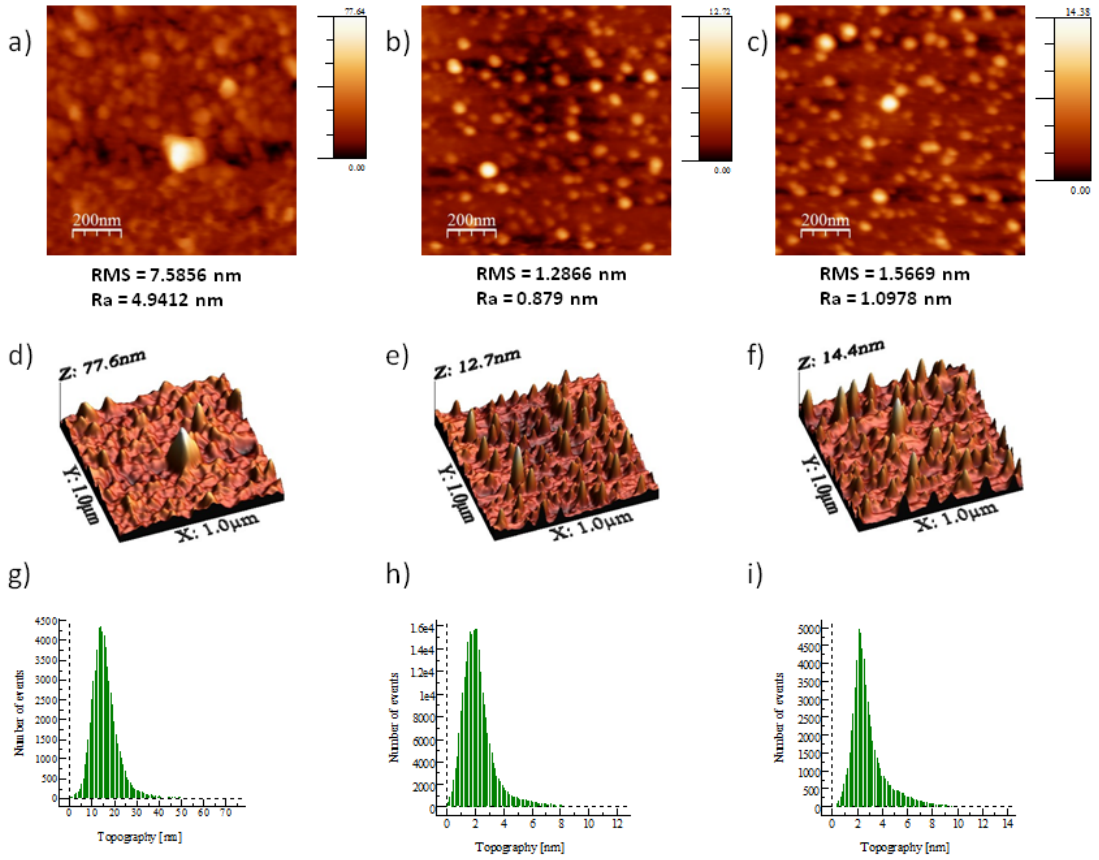

Figure A3. AFM analysis of three areas of Si 100 surface coated with 50 mM concentrated solution of EP in toluene at 80 °C with Pt catalyst. The topography of the first area is depicted in images a), d) and g) showing the 2D image (x, y direction); the 3D image and a histogram based on which the surface roughness was estimated. Similar analysis was conducted for all areas. The surface roughness is shown under subfigures a), b), and c). An average of the RMS (R_q) roughnesses is shown in Table 5. The R_a is surface roughness calculated using different formula and is shown for completion.

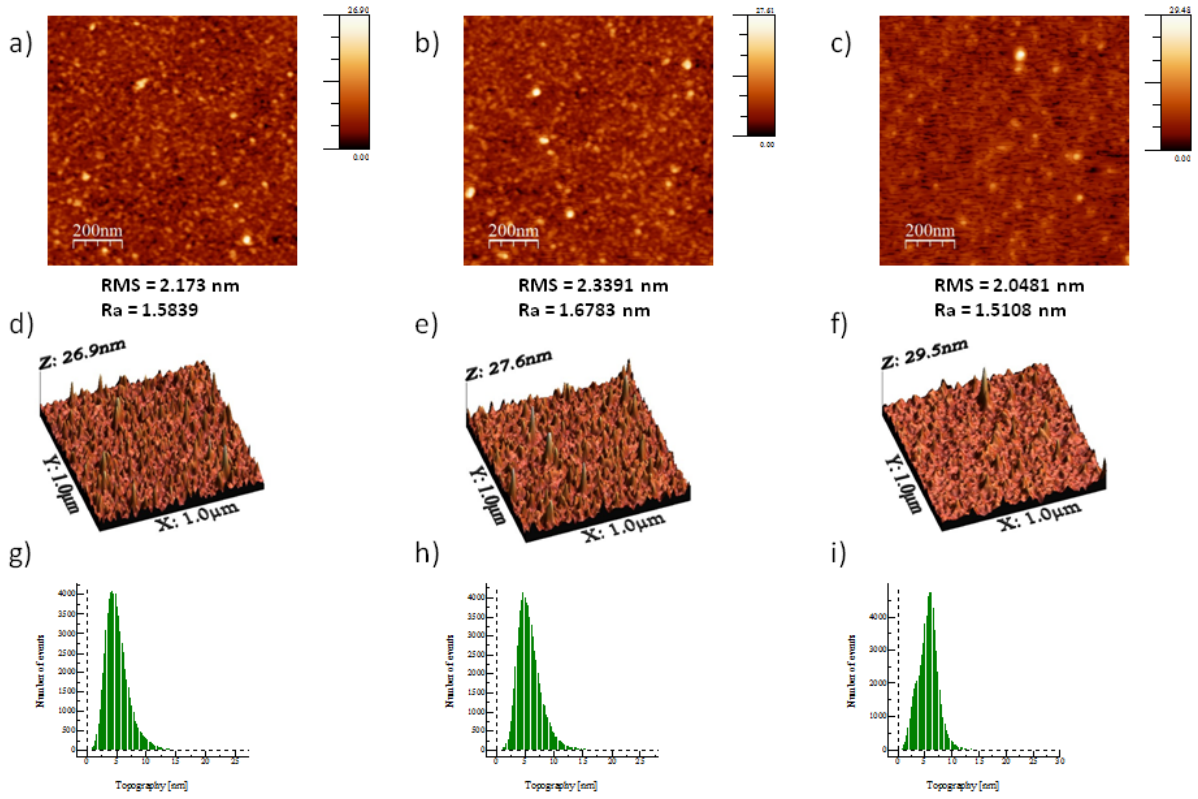

Figure A4. AFM analysis of two areas of Si 100 surface coated with 50 mM concentrated solution of VP in toluene at 80 °C with Pt catalyst. Three areas were imaged. The topography of the first area is depicted in images a), d) and g) showing the 2D image (x, y direction); the 3D image and a histogram based on which the surface roughness was estimated. Similar analysis was conducted for all areas. The surface roughness is shown under subfigures a), b), and c). An average of the RMS (R_q) roughnesses is shown in Table 5. The R_a is surface roughness calculated using different formula and is shown for completion.

References

[1] . J. M. Martinis et. al. Phys. Rev. Lett. 95, 210503 (2005)

[2] E. Lock et. al. [in preparation]

[3] B. Sarabi et. al.. arXiv: 1501.0565v3{cond-mat.supr.com} 5 Apr. 2016

[4] M. Khalil et. al. Phys. Rev. B 90, 100201R (2014)

[5] A. B. Sieval et. al. Langmuir 14, 1759 (1998)

[6] S. Pujari et. al. Langmuir 29, 570-580 (2013)

[7] Q. Sun et. al. Angew. Chem. Int. Ed. 43, 1352 (2004)

[8] T. Alves et. al. Phys. Chem. Chem. Phys. 18, 8945 (2016)

[9] K. Utzat et. al. J. Phys. Chem. A 114, 6913 (2010)